

This copy is for your personal, non-commercial use only.

If you wish to distribute this article to others, you can order high-quality copies for your colleagues, clients, or customers by [clicking here](#).

Permission to republish or repurpose articles or portions of articles can be obtained by following the guidelines [here](#).

The following resources related to this article are available online at www.sciencemag.org (this information is current as of June 2, 2010):

Updated information and services, including high-resolution figures, can be found in the online version of this article at:

<http://www.sciencemag.org/cgi/content/full/328/5977/483>

Supporting Online Material can be found at:

<http://www.sciencemag.org/cgi/content/full/science.1184741/DC1>

This article **cites 28 articles**, 9 of which can be accessed for free:

<http://www.sciencemag.org/cgi/content/full/328/5977/483#otherarticles>

This article has been **cited by** 1 article(s) on the ISI Web of Science.

This article has been **cited by** 1 articles hosted by HighWire Press; see:

<http://www.sciencemag.org/cgi/content/full/328/5977/483#otherarticles>

This article appears in the following **subject collections**:

Planetary Science

http://www.sciencemag.org/cgi/collection/planet_sci

volumetric capacitance is similar to what was measured on a ~300- μm -thick traditionally processed electrode (~80 F/cm³).

As the coating thickness decreases to ~2 μm , the volumetric capacitance increases to nearly 180 F/cm³ in TEABF₄ electrolyte and ~160 F/cm³ in 1M H₂SO₄. The spacing between cracks is larger than the film thickness (Fig. 3B); thus, electrolyte transport is controlled by the transport from bulk electrolyte to the current collector through the entire film thickness, making crack influence on capacitance marginal at best. Also, the crack volume in comparison with the pore volume of the CDC layer (>50%) does not lead to a substantial increase in electrolyte volume or electrode surface area (<1%). Simply removing ~50% of empty volume between particles in traditional electrodes would provide volumetric capacitance numbers of ~100 F/cm³ in organic electrolyte and ~160 F/cm³ in sulfuric acid electrolyte; it is believed that this is the major reason for the thin-film results. The extremely intimate contact between the underlying current collector and CDC film would also facilitate good electron transfer into the film, limiting the voltage drop through this interface and resulting in higher charge compensation in the double-layer, which could explain capacitance values above what is expected based solely on sphere-packing assumptions. The decrease in capacitance with thicker films is most likely due to microstructural rearrangement from surface stresses relaxing, which results in porosity collapse and perturbation of the interconnected structure that facilitates electron conduction. The effects of electrolyte starvation with thicker films coupled to structure collapse may also play a role in the drop in capacitance values [as previously shown by Zheng *et al.* (28)], with thicker films requiring a larger number of

ions to migrate from the bulk electrolyte into the pore structure.

Although we observed microcracking in the TiC-CDC films in this study, it has previously been shown that dense coatings can be made to 200- μm thickness for SiC-CDC films (29). Earlier work chlorinating sputtered amorphous TiC, which is the simplest method for patterning carbide substrates for micro-supercapacitors on devices, has shown that TiC-CDC can also be produced crack-free, at least in the form of 0.5- μm films (21). Therefore, in terms of extrapolating these results to realizable micro-supercapacitors, we expect that what may be viewed as technological hurdles should, in fact, lead to better-functioning devices.

References and Notes

- J. W. Long, B. Dunn, D. R. Rolison, H. S. White, *Chem. Rev.* **104**, 4463 (2004).
- M. Armand, J. M. Tarascon, *Nature* **451**, 652 (2008).
- P. Simon, Y. Gogotsi, *Nat. Mater.* **7**, 845 (2008).
- J. Miller, A. F. Burke, *Electrochem. Soc. Interface* **17** (Spring), 53 (2008).
- R. J. Brodd *et al.*, *J. Electrochem. Soc.* **151**, K1 (2004).
- D. Linden, Ed., *Handbook of Batteries* (McGraw-Hill, New York, ed. 2, 2001).
- A. Tanimura, A. Kovalenko, F. Hirata, *Chem. Phys. Lett.* **378**, 638 (2003).
- B. W. Ricketts, C. Ton-That, *J. Power Sources* **89**, 64 (2000).
- A. S. Arico, P. Bruce, B. Scrosati, J.-M. Tarascon, W. van Schalkwijk, *Nat. Mater.* **4**, 366 (2005).
- V. L. Pushparaj *et al.*, *Proc. Natl. Acad. Sci. U.S.A.* **104**, 13574 (2007).
- S. W. Lee, B.-S. Kim, S. Chen, Y. Shao-Horn, P. T. Hammond, *J. Am. Chem. Soc.* **131**, 671 (2009).
- D. Pech *et al.*, *J. Power Sources* **195**, 1266 (2010).
- W. Sun, X. Y. Chen, *Microelectron. Eng.* **86**, 1307 (2009).
- J. Wang, J. Polleux, J. Lim, B. Dunn, *J. Phys. Chem. C* **111**, 14925 (2007).
- M. Kaempgen, C. K. Chan, J. Ma, Y. Cui, G. Gruner, *Nano Lett.* **9**, 1872 (2009).
- K. Naoi, M. Morita, *Electrochem. Soc. Interface* **17** (Spring), 44 (2008).
- H. J. Ahn, W. B. Kim, T. Y. Seong, *Electrochem. Commun.* **10**, 1284 (2008).
- M. J. Lee *et al.*, *J. Electroceram.* **17**, 639 (2006).
- J. Leis, M. Arulepp, A. Kuura, M. Latt, E. Lust, *Carbon* **44**, 2122 (2006).
- A. Jänes, E. Lust, *J. Electrochem. Soc.* **153**, A113 (2006).
- E. N. Hoffman, G. Yushin, B. G. Wandler, M. W. Barsoum, Y. Gogotsi, *Mater. Chem. Phys.* **112**, 587 (2008).
- R. K. Dash, G. Yushin, Y. Gogotsi, *Microporous Mesoporous Mater.* **86**, 50 (2005).
- Z. G. Cambaz, G. N. Yushin, Y. Gogotsi, K. L. Vysnyakova, L. N. Pereselenyeva, *J. Am. Ceram. Soc.* **89**, 509 (2006).
- J. Chmiola, C. Largeot, P. L. Taberna, P. Simon, Y. Gogotsi, *Angew. Chem. Int. Ed.* **47**, 3392 (2008).
- J. Chmiola *et al.*, *Science* **313**, 1760 (2006); published online 17 August 2006 (10.1126/science.1132195).
- R. Lin *et al.*, *J. Electrochem. Soc.* **156**, A7 (2009).
- R. Mysyk, E. Raymundo-Pinero, F. Beguin, *Electrochem. Commun.* **11**, 554 (2009).
- J. P. Zheng, J. Huang, T. R. Jow, *J. Electrochem. Soc.* **144**, 2417 (1997).
- D. A. Ersoy, M. J. McNallan, Y. Gogotsi, *Mater. Res. Innovations* **5**, 55 (2001).
- Electron microscopy and Raman spectroscopy analyses were conducted with the use of instruments in the Centralized Research Facility of the College of Engineering, Drexel University and Université Paul Sabatier de Toulouse. J.C. was supported by Integrative Graduate Education and Research Traineeship (IGERT) and Graduate Research fellowships from the NSF, C.L. was supported by Délégation Générale pour l'Armement, and Y.G. was supported by the U.S. Department of Energy, Office of Basic Energy Sciences, Division of Materials Sciences and Engineering under award ER46473. Collaboration between the participating universities was supported by a Partnership University Fund grant. Y.G. is also Founder and Chief Science Officer, Y-Carbon. The authors also have a related patent application no. 61/025058.

Supporting Online Material

www.sciencemag.org/cgi/content/full/328/5977/480/DC1
Materials and Methods
Fig. S1

2 November 2009; accepted 9 March 2010
10.1126/science.1184126

Constraints on the Formation Age of Cometary Material from the NASA Stardust Mission

J. E. P. Matzel,^{1,2*} H. A. Ishii,¹ D. Joswiak,³ I. D. Hutcheon,^{1,2} J. P. Bradley,¹ D. Brownlee,³ P. K. Weber,² N. Teslich,¹ G. Matrajt,³ K. D. McKeegan,⁴ G. J. MacPherson⁵

We measured the ²⁶Al-²⁶Mg isotope systematics of a ~5-micrometer refractory particle, Coki, returned from comet 81P/Wild 2 in order to relate the time scales of formation of cometary inclusions to their meteoritic counterparts. The data show no evidence of radiogenic ²⁶Mg and define an upper limit to the abundance of ²⁶Al at the time of particle formation: ²⁶Al/²⁷Al < 1 × 10⁻⁵. The absence of ²⁶Al indicates that Coki formed >1.7 million years after the oldest solids in the solar system, calcium- and aluminum-rich inclusions (CAIs). The data suggest that high-temperature inner solar system material formed, was subsequently transferred to the Kuiper Belt, and was incorporated into comets several million years after CAI formation.

The Stardust mission to comet 81P/Wild 2 was designed around the premise that comets preserve pristine remnants of the material from which the solar system formed; in

2006, Stardust returned the first samples from a comet. The mission was expected to provide a unique window into the early solar system by returning a mix of solar system condensates,

amorphous grains from the interstellar medium, and true stardust (crystalline grains originating in distant stars). Initial results, however, indicate that Wild 2 instead contains an abundance of high-temperature silicate and oxide minerals analogous to minerals in carbonaceous chondrites (1–5). The detection of Wild 2 particles that resemble calcium- and aluminum-rich inclusions (CAIs) (6) is particularly noteworthy because CAIs were most plausibly created within 1 AU of the infant Sun (7) and are the oldest objects formed in the solar nebula (8). The presence of inner solar system material in Wild 2 (1–3, 9) underscores the importance of radial transport of material

¹Institute of Geophysics and Planetary Physics, Lawrence Livermore National Laboratory, Livermore, CA 94550, USA.

²Glenn T. Seaborg Institute, Lawrence Livermore National Laboratory, Livermore, CA 94550, USA. ³Department of Astronomy, University of Washington, Seattle, WA 98195, USA. ⁴Department of Earth and Space Sciences, University of California, Los Angeles, CA 90095, USA. ⁵Department of Mineral Sciences, National Museum of Natural History, MRC-119, Smithsonian Institution, Washington, DC 20560, USA.

*To whom correspondence should be addressed. E-mail: matzel2@llnl.gov

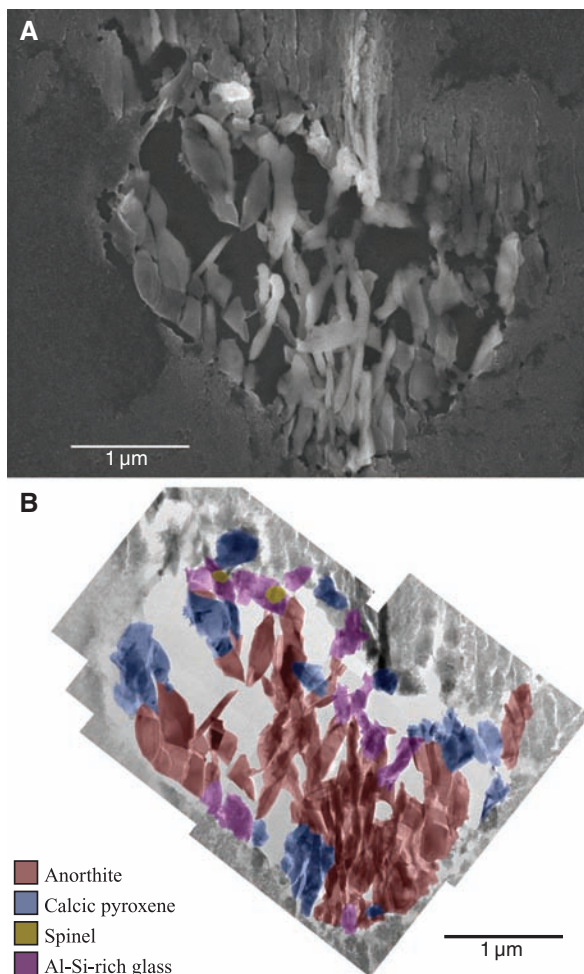


Fig. 1. (A) Secondary electron image of the Coki section analyzed in this study, showing mineral shards surrounded by compressed aerogel. (B) Corresponding false-color mineral map overlaid on a montage of bright-field TEM images (13).

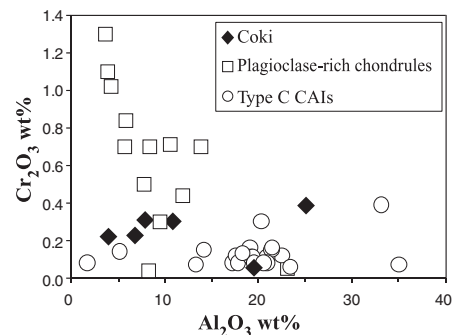


Fig. 2. Coki pyroxene chemical compositions as compared to type C CAIs (15, 16) and plagioclase-rich chondrules (14, 16, 33).

Table 1. ^{26}Al - ^{26}Mg isotopic data from Coki. Uncertainties are two standard deviations.

Sample	$^{27}\text{Al}/^{24}\text{Mg}$	$\delta^{26}\text{Mg}$ (‰)*
Coki 1†	342 ± 34	-17 ± 37
Coki 2‡	150 ± 15	18 ± 45
Coki 3§	6.9 ± 0.7	1.6 ± 6.5

*Per mil deviation in $^{26}\text{Mg}/^{24}\text{Mg}$ relative to terrestrial Mg after correction for mass-dependent fractionation. See (13) for details. †Includes pixels with $^{27}\text{Al}/^{24}\text{Mg} > 200$. ‡Includes pixels with $^{27}\text{Al}/^{24}\text{Mg}$ between 100 and 200. §Includes pixels with $^{27}\text{Al}/^{24}\text{Mg} < 10$.

over large distances in the early solar nebula, and it raises key questions regarding the time scale of formation of comets and the relationship between Wild 2 and other primitive solar nebula objects.

With a half-life of 730,000 years, the decay of the short-lived radionuclide ^{26}Al to ^{26}Mg provides a high-resolution relative chronometer for events occurring during the first several million years of solar system history. Assuming a homogeneous initial distribution of ^{26}Al within the solar nebula (10), differences in the inferred initial $^{26}\text{Al}/^{27}\text{Al}$ can be ascribed to the passage of time. Most CAIs contain radiogenic ^{26}Mg as a result of the in situ decay of ^{26}Al (10). CAIs that contain little to no radiogenic ^{26}Mg fall primarily into two categories: (i) highly refractory grains [e.g., (11)] and rare FUN inclusions named for their fractionation and unidentified nuclear isotopic effects, which are believed to have formed very early (12); and (ii) CAIs that show clear petrographic evidence for later reprocessing (10).

We applied the ^{26}Al - ^{26}Mg isotope system to a recently discovered refractory particle from Wild 2 (C2061,3,141,0,0; hereafter Coki). Coki contains no detectable radiogenic ^{26}Mg , strongly suggestive of late formation at least 1.7 million years after most CAIs. The ^{26}Al - ^{26}Mg data from

Coki provide an important constraint on the accretion time scale of comets such as Wild 2 and the timing of radial mixing of thermally processed, high-temperature materials from the inner solar system to the outer reaches of the solar nebula.

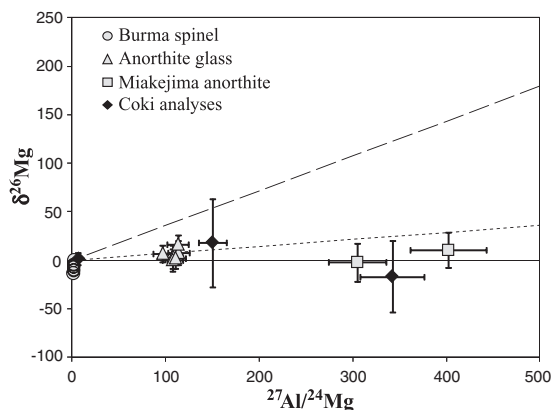
Coki is a polycrystalline refractory particle ~ 5 μm in diameter, likely a fragment of a once much larger particle (13); it is composed mostly of anorthite with minor calcic pyroxene and an Al-Si-rich glass occurring around the edge of the particle (Fig. 1). The glass may be due to melting experienced by the particle during capture into the Stardust silica aerogel collector. Small (< 200 nm) spinel crystals are enclosed in glass and anorthite. The abundance of anorthite and absence of melilite (either within the Coki particle or anywhere along its deceleration track) suggest that Coki most closely resembles a minor class of CAIs (type C) or plagioclase-rich chondrules (6, 14, 15). Coki pyroxene compositions are Ti-rich and Fe- and Cr-poor (Fig. 2, fig. S1, and table S1) relative to pyroxene commonly found in plagioclase-rich chondrules [e.g., (14)], which suggests that Coki may be most comparable to type C CAIs. Both type C CAIs and plagioclase-rich chondrules show clear petrographic evidence for complex multistage histories, including melting of refractory precursor materials and assim-

ilation of late-stage metamorphic minerals in the chondrite-forming region (6, 14–16).

We used a secondary ion mass spectrometer with nanometer-scale spatial resolution, the Cameca NanoSIMS 50, to measure the Mg isotope composition of Coki anorthite. An electron-transparent section, ~ 3 μm in diameter and 0.1 μm thick, was first mapped by transmission electron microscopy energy-dispersive spectroscopy (TEM/EDS) (13) (Fig. 1). The section was then prepared for NanoSIMS analysis with the use of a focused ion beam instrument to deposit a Pt support film behind the Coki section and to remove interfering Mg-rich minerals (13). We simultaneously collected four ion images corresponding to $^{24}\text{Mg}^+$, $^{25}\text{Mg}^+$, $^{26}\text{Mg}^+$, and $^{27}\text{Al}^+$ secondary ions. The ion images were subdivided into three spatially continuous regions on the basis of $^{27}\text{Al}/^{24}\text{Mg}$ ratio, and Mg isotope ratios were calculated by summing the total ion intensity of each isotope over each region (13) (Table 1).

The Mg isotope composition of Coki anorthite is indistinguishable from that of the terrestrial plagioclase standards. We found no evidence in Coki for either radiogenic ^{26}Mg from the decay of ^{26}Al or mass-dependent fractionation of Mg isotopes (Table 1 and Fig. 3). The upper limit for the initial abundance of ^{26}Al at the time Coki crystallized is $^{26}\text{Al}/^{27}\text{Al} < 1 \times 10^{-5}$, according to the 2σ upper bound to the slope of a line fitted to the data. The absence of substantial mass-dependent fractionation of Mg isotopes indicates that Coki is not a member of the rare group of CAIs known as FUN inclusions (12).

Fig. 3. ^{26}Al - ^{26}Mg evolution diagram for Coki. The solid horizontal line corresponds to terrestrial Mg. The dashed line indicates the canonical $^{26}\text{Al}/^{27}\text{Al}$ value of 5×10^{-5} ; the dotted line represents the 2σ upper error bound on a line fitted to the data and forced through the origin corresponding to initial $^{26}\text{Al}/^{27}\text{Al} < 1 \times 10^{-5}$.



The ^{26}Al - ^{26}Mg isotope systematics of primitive solar system materials establish a framework for the interpretation of the Coki Al-Mg data. The initial abundance of ^{26}Al in CAIs provides the anchor point for the ^{26}Al - ^{26}Mg chronometer; the ^{26}Al - ^{26}Mg record of CAIs and chondrules is best explained by formation in an isotopically homogeneous nebular reservoir characterized by an initial $^{26}\text{Al}/^{27}\text{Al}$ ratio of $\sim 5 \times 10^{-5}$ (10). Recent high-precision studies of ^{26}Al in CAIs (17, 18) and chondrules (19) support the inference of a uniform initial distribution of $^{26}\text{Al}/^{27}\text{Al}$ in the solar nebula and a very short time interval (<20,000 years) for the primary crystallization of CAIs. Type C CAIs and chondrules, with initial $^{26}\text{Al}/^{27}\text{Al}$ ratios of $\ll 5 \times 10^{-5}$, typically show textural and mineralogical evidence for extensive melting of precursor materials [e.g., (20)], consistent with the absence of ^{26}Al . The ^{26}Al - ^{26}Mg record of plagioclase-rich chondrules indicates that the time interval between CAI formation and the onset of chondrule formation is ~ 1 million years (21, 22) and that transient events capable of producing high-temperature nebular components in the inner solar system persisted for close to 4 million years (23–25).

Our determination that Coki formed with an initial $^{26}\text{Al}/^{27}\text{Al}$ of $< 1 \times 10^{-5}$ indicates that Coki crystallized at least 1.7 million years after the onset of CAI formation. This value is consistent with data for type C CAIs and plagioclase-rich chondrules that typically yield initial $^{26}\text{Al}/^{27}\text{Al} \leq 1 \times 10^{-5}$ [(23) and references therein; (26)]. The lack of ^{26}Al in some highly refractory phases [e.g., hibonite (11)] has been interpreted as very early formation prior to the incorporation or homogenization of ^{26}Al in the accretion disk. However, the petrography and mineral composition of Coki are inconsistent with formation as very early condensates. The lack of ^{26}Al in Coki is also unlikely to be attributable to later redistribution of radiogenic ^{26}Mg either on Wild 2 or during capture in aerogel. The poorly consolidated and fine-grained nature of the material collected from Wild 2 indicates that it had not been lithified and altered in Wild 2 by internal processes such as heating, compaction, or aqueous alteration

(3). Although all particles were modified to some degree by capture in aerogel, particles that are larger than $1 \mu\text{m}$, such as Coki, are typically well preserved and appear to have been protected by their own thermal inertia (3). We estimate that the distance over which Mg diffused in anorthite [using the diffusion coefficient of (27)] during the conditions of capture in aerogel [i.e., $T \approx 2000 \text{ K}$, $t > 1 \mu\text{s}$ (3)] is less than 1 nm .

We postulate that Coki formed by melting of solid precursor materials during transient high-temperature events in the inner solar system, analogous to the formation of type C CAIs and chondrules (20, 28). The chemical and isotopic data suggest that Coki is transitional between the only other CAI-like particle described from Wild 2, named Inti (1, 3, 9), and the chondrule-like objects from Wild 2 described by Nakamura *et al.* (2). As such, Coki may provide a direct link between primary CAI formation and later chondrule formation. Inti closely resembles type B CAIs in its mineralogy and ^{16}O -rich isotope composition (1, 9), whereas the ferromagnesian chondrule-like objects have less refractory chemical compositions and display a range of O-isotope compositions suggesting that they experienced oxygen isotope exchange in a ^{16}O -depleted reservoir (2). These observations lead to the conclusion made in previous studies (1–4) that Wild 2 contains an abundance of chemically and thermally processed high-temperature material from the inner solar system. In this sense, Wild 2 is analogous to carbonaceous chondrite meteorites (5).

As an additional member of the collection of refractory materials from Wild 2, Coki adds weight to the evidence suggesting that high-temperature silicate and oxide mineral assemblages formed close to the Sun and were subsequently transported to the region of comet accretion. Coki provides a temporal constraint demonstrating that refractory material supplied to the Kuiper Belt crystallized at least 1.7 million years after the onset of CAI formation. This observation in turn requires transport of inner solar system material to the outer reaches of the solar system at distances exceeding 30 AU and incorporation into cometary bodies over an extended period of at

least several million years. Outward transport of Coki to the Kuiper Belt must have occurred as late as (if not later than) the time over which chondritic meteorites and the oldest differentiated meteorites formed [see (29)]. The age constraint derived from Coki indicates that the transport mechanisms that supplied high-temperature inner solar system material to the outer reaches of the solar nebula—whether by lofting above the disk in an X-wind model (30) or via mixing processes within the solar nebula [e.g., (31, 32)]—operated over a time scale of > 2 million years as solids settled to the mid-plane and the disk evolved.

References and Notes

1. K. D. McKeegan *et al.*, *Science* **314**, 1724 (2006).
2. T. Nakamura *et al.*, *Science* **321**, 1664 (2008).
3. D. Brownlee *et al.*, *Science* **314**, 1711 (2006).
4. M. E. Zolensky *et al.*, *Science* **314**, 1735 (2006).
5. H. A. Ishii *et al.*, *Science* **319**, 447 (2008).
6. G. J. MacPherson, in *Meteorites, Comets and Planets: Treatise on Geochemistry, Volume 1*, A. M. Davis, Ed. (Elsevier, Amsterdam, 2005), pp. 201–245.
7. K. D. McKeegan, M. Chaussidon, F. Robert, *Science* **289**, 1334 (2000).
8. Y. Amelin, A. N. Krot, I. D. Hutcheon, A. A. Ulyanov, *Science* **297**, 1678 (2002).
9. S. B. Simon *et al.*, *Meteorit. Planet. Sci.* **43**, 1861 (2008).
10. G. J. MacPherson, A. M. Davis, E. K. Zinner, *Meteoritics* **30**, 365 (1995).
11. M.-C. Liu *et al.*, *Geochim. Cosmochim. Acta* **73**, 5051 (2009).
12. G. J. Wasserburg, T. Lee, D. A. Papanastassiou, *Geophys. Res. Lett.* **4**, 299 (1977).
13. See supporting material on Science Online.
14. G. J. MacPherson, G. R. Huss, *Geochim. Cosmochim. Acta* **69**, 3099 (2005).
15. D. A. Wark, *Geochim. Cosmochim. Acta* **51**, 221 (1987).
16. A. N. Krot *et al.*, *Geochim. Cosmochim. Acta* **71**, 4342 (2007).
17. K. Thrane, M. Bizzarro, J. A. Baker, *Astrophys. J.* **646**, L159 (2006).
18. B. Jacobsen *et al.*, *Earth Planet. Sci. Lett.* **272**, 353 (2008).
19. J. Villeneuve, M. Chaussidon, G. Libourel, *Science* **325**, 985 (2009).
20. A. N. Krot, H. Yurimoto, I. D. Hutcheon, G. J. MacPherson, *Nature* **434**, 998 (2005).
21. N. T. Kita, H. Nagahara, S. Togashi, Y. Morishita, *Geochim. Cosmochim. Acta* **64**, 3913 (2000).
22. G. R. Huss, G. J. MacPherson, G. J. Wasserburg, S. S. Russell, G. Srinivasan, *Meteorit. Planet. Sci.* **36**, 975 (2001).
23. I. D. Hutcheon, K. K. Marhas, A. N. Krot, J. N. Goswami, R. H. Jones, *Geochim. Cosmochim. Acta* **73**, 5080 (2009).
24. S. S. Russell *et al.*, in *Meteorites and the Early Solar System II*, D. S. Lauretta, H. Y. McSween Jr., Eds. (Univ. of Arizona Press, Tucson, AZ, 2006), pp. 233–251.
25. E. R. D. Scott, A. N. Krot, in *Chondrites and the Protoplanetary Disk*, A. N. Krot, E. R. D. Scott, B. Reipurth, Eds. (Astronomical Society of the Pacific, San Francisco, 2005), pp. 15–53.
26. A. N. Krot *et al.*, *Meteorit. Planet. Sci.* **42**, 1197 (2007).
27. T. LaTourrette, G. J. Wasserburg, *Earth Planet. Sci. Lett.* **158**, 91 (1998).
28. R. H. Jones, T. Lee, H. C. Connolly Jr., S. G. Love, H. Shang, in *Protostars and Planets IV*, V. Mannings, A. P. Boss, S. S. Russell, Eds. (Univ. of Arizona Press, Tucson, AZ, 2000), pp. 927–962.
29. R. W. Carlson, M. Boyet, *Earth Planet. Sci. Lett.* **279**, 147 (2009).

30. F. H. Shu, H. Shang, T. Lee, *Science* **271**, 1545 (1996).
 31. F. J. Ciesla, *Science* **318**, 613 (2007).
 32. A. P. Boss, *Astrophys. J.* **616**, 1265 (2004).
 33. Y. J. Sheng, I. D. Hutcheon, G. J. Wasserburg, *Geochim. Cosmochim. Acta* **55**, 581 (1991).
 34. This work was performed under the auspices of the U.S. Department of Energy by Lawrence Livermore National Laboratory (LLNL) under contract DE-AC52-

07NA27344. Supported by NASA grants NNH07AG461 (H.A.I.) and NNH04AB471 (I.D.H.) and by LLNL grant 06-ERI-001 (J.P.B.).

Supporting Online Material

www.sciencemag.org/cgi/content/full/science.1184741/DC1
 Materials and Methods
 SOM Text

Figs. S1 to S3
 Tables S1 to S3
 References

16 November 2009; accepted 16 February 2010
 Published online 25 February 2010;
 10.1126/science.1184741
 Include this information when citing this paper.

Asian Monsoon Failure and Megadrought During the Last Millennium

Edward R. Cook,^{1*} Kevin J. Anchukaitis,¹ Brendan M. Buckley,¹ Rosanne D. D'Arrigo,¹ Gordon C. Jacoby,¹ William E. Wright^{1,2}

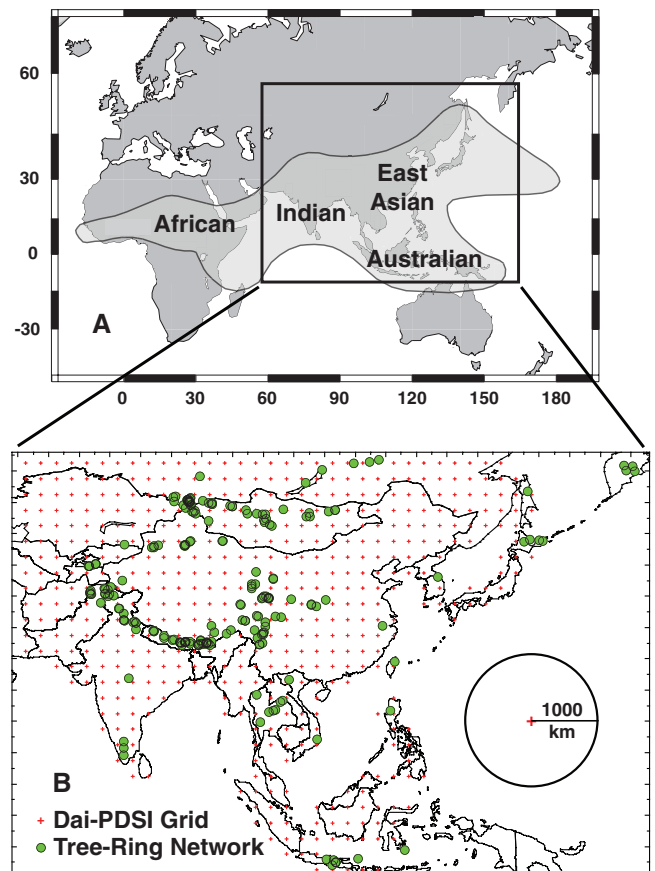
The Asian monsoon system affects more than half of humanity worldwide, yet the dynamical processes that govern its complex spatiotemporal variability are not sufficiently understood to model and predict its behavior, due in part to inadequate long-term climate observations. Here we present the Monsoon Asia Drought Atlas (MADA), a seasonally resolved gridded spatial reconstruction of Asian monsoon drought and pluvials over the past millennium, derived from a network of tree-ring chronologies. MADA provides the spatiotemporal details of known historic monsoon failures and reveals the occurrence, severity, and fingerprint of previously unknown monsoon megadroughts and their close linkages to large-scale patterns of tropical Indo-Pacific sea surface temperatures. MADA thus provides a long-term context for recent monsoon variability that is critically needed for climate modeling, prediction, and attribution.

Monsoon failures, megadroughts, and extreme flooding events have repeatedly affected the agrarian peoples of Asia over the past millennium. Despite its critical importance to human populations and ecosystems, not enough is known about the long-term spatiotemporal variability of the Asian monsoon to explain the complex mechanisms that drive its variability. A scarcity of long-term instrumental climate data for many remote regions of Monsoon Asia (1) (fig. S1) impedes progress toward resolving these issues. In addition, global climate models fail to accurately simulate the Asian monsoon (2) and related tropical Indo-Pacific forcings (3), and these limitations have hampered our ability to plan for future, potentially rapid and nonlinear, hydroclimatic shifts in a warming world. Under such warming, Monsoon Asia appears to be particularly vulnerable (4, 5).

To better elucidate the spatial complexity of the Asian monsoon (Fig. 1A), a large-scale, spatially explicit, long-term data set is needed. Such a long-term perspective is essential both for validation of climate models and for integration and comparison with other proxy, historical, and archaeological data. This context is provided here by our Monsoon Asia Drought Atlas (MADA), which offers an absolutely dated, annually resolved reconstruction of Asian monsoon spatio-

temporal variability over the past thousand years. The MADA provides a seasonal- to centennial-scale window into the Asian monsoon's repeated

Fig. 1. (A) Map showing the complex regional expressions of the monsoon over Africa, India, East Asia, and south into northern Australia [redrawn from (11)], with the overall MADA domain enclosed by the interior black rectangle. The MADA domain limits cover all but the African portion of the greater monsoon system. (B) More detailed view of the MADA domain; the 534 grid points of instrumental PDSIs (13) (red crosses) were reconstructed by the 327-series tree-ring chronology network (1) (green dots). Contributors to the development of this tree-ring network are listed in table S1 (1).



¹Tree-Ring Laboratory, Lamont-Doherty Earth Observatory of Columbia University, Palisades, NY 10964, USA. ²School of Forestry and Natural Resources, National Taiwan University, Taipei 10617, Taiwan.

*To whom correspondence should be addressed. E-mail: drdendro@ldeo.columbia.edu